Advanced Optical Materials

ADVANCED OPTICAL MATERIALS
www.advopticalmat.de

RESEARCH ARTICLE OPEN ACCESS

GeSn Quantum Wells for Room-Temperature Mid-Infrared Lasing on Si and on Insulator Platforms

Antoine Meyer[1] | Hector-Mauricio Reynoso-de la Cruz[1] | Omar Concepción[2] | Prateek Kaul[2] | Konstantinos Pantzas[1] | Etienne Herth[1] | Z. Ikonic[3] | Giovanni Capellini[4,5] | Detlev Grützmacher[2] | Moustapha El Kurdi[1,6] | Dan Buca[2]

[1]C2N, CNRS, Universite Paris-Saclay, Palaiseau, France | [2]Peter Gruenberg Institute-9, Semiconductor Nanoelectronics and JARA-Fundamentals of Future Information Technologies, Forschungszentrum Juelich, Juelich, Germany | [3]Pollard Institute, School of Electronic and Electrical Engineering, University of Leeds, Leeds, UK | [4]IHP–Leibniz Institut Für Innovative Mikroelektronik, Frankfurt (Oder), Germany | [5]Department of Sciences, Università Roma Tre, Roma, Italy | [6]LTCI, Télécom Paris, Institut Polytechnique de Paris, Palaiseau, France

Correspondence: Moustapha El Kurdi (moustapha.elkurdi@telecom-paris.fr) | Dan Buca (d.m.buca@fz-juelich.de)

Received: 8 January 2026 | **Revised:** 9 June 2026 | **Accepted:** 12 June 2026

ABSTRACT

Recent advances in group-IV materials, particularly germanium–tin (GeSn) alloys, have reinvigorated the pursuit of CMOS-compatible light sources. The optical performance of GeSn is governed by the coupled effects of Sn composition and lattice strain, which together dictate optical gain and the maximum operating temperature. Here, through a tailored heterostructure design and epitaxial strategy, we realize GeSn multi-quantum-well (MQW) heterostructures with ∼15 at.% Sn in the wells and systematically investigate their performance on two distinct platforms: GeSn on-Si bulk and GeSn-on-insulator. By engineering the lattice strain from compressive to tensile, we reveal the fundamental trade-off between lasing threshold and maximum operating temperature. The GeSn-on-insulator MQW platform delivers outstanding performance, enabling mid-infrared lasing at room temperature (293 K) with a threshold of 500 kW cm^{-2} in a simple mesa cavity, while the tensile-strained counterpart achieves a lower threshold of 8 kW cm^{-2} at 77 K but sustains laser emission only up to 265 K. These results indicate that GeSn MQWs are a viable group-IV gain medium for mid-infrared lasing and highlight their potential for integration into CMOS-compatible silicon photonic circuits.

1 | Introduction

Group-IV photonics has advanced rapidly over the past decade, emerging as a promising platform for integrating optical components with CMOS-compatible processes [1, 2]. The advent of direct-bandgap GeSn alloys opens new pathways for AI-accelerated sensing and in-memory optical computing [3, 4], where information processing and storage occur directly within the photonic domain. Leveraging their mid-infrared operation, GeSn devices could enable intelligent edge computing functionalities—such as real-time spectral analysis, chemical detection, and adaptive optical response—crucial for edge AI and neuromorphic systems [5].

GeSn alloys have also emerged as efficient gain media for Si-compatible lasers. Their epitaxial growth on Ge/Si virtual substrates [6, 7] overcomes the limitations of indirect-bandgap group-IV semiconductors through compositional tuning and strain engineering. Mid-infrared lasing has been demonstrated under pulsed [8, 9] and continuous-wave optical pumping [10], confirming their potential for on-chip light sources. Their tunable band structure and CMOS compatibility make GeSn a versatile platform for short- and mid-wave infrared (λ = 2–5 µm) emission, complementing III–V semiconductors for sensing [11, 12], lab-on-a-chip technologies [13] and integrated photonics applications.

Lasing has been demonstrated across a wide range of Sn compositions and cavity geometries, including microdisks [8, 14], ridge waveguides [15, 16], photonic crystal resonators [17] and even nanowire [18]. However, achieving low-threshold operation at room temperature remains challenging. High Sn concentrations are required to ensure sufficient Γ–L valley separation (>100 meV), enhancing direct-bandgap character and suppressing intervalley scattering [10]. At the same time, higher Sn content degrades crystalline quality, increases non-radiative recombination and optical losses, and introduces compressive strain that promotes defects and limits thermal stability.

To address these limitations, layer-transfer techniques have been adapted to GeSn-on-insulator (GeSnOI) platforms [9, 10, 19, 20]. This approach removes the defective GeSn/Ge interface and enables integration of functional interlayers such as thermal sinks or stressor layers. Biaxial tensile strain can mimic higher Sn incorporation while preserving crystal quality, reducing the carrier density required for population inversion and lowering thresholds. Nevertheless, the tradeoff with Sn content remains evident: the optically pumped threshold at 5 K is ~1 kW cm^{-2} tensile-strained $Ge_{0.95}Sn_{0.05}$ layer [10], compared with 12 kW cm^{-2} for $Ge_{0.86}Sn_{0.14}$ [9]. Higher Sn content also increases the maximum operating temperature from 100 to 295 K, highlighting the balance between optical gain and material robustness.

Progress in Sn-based epitaxy has enabled the growth of high-quality GeSn multi-quantum-well (MQW) heterostructures [8, 21–25], employing binary GeSn wells and Ge or ternary SiGeSn barriers. The MQW design significantly enhances optical confinement and gain, resulting in a pronounced reduction of the lasing threshold. However, the maximum lasing temperature remains limited to ~ 150 K. This limitation arises partly from the limited stoichiometric control achievable with current epitaxial techniques and from uncertainties in key material parameters that influence band-structure calculations and, consequently, the optimization of the structure through modeling. Furthermore, short-range ordering phenomena recently observed in the lattice of SiGeSn alloys [26–28] add another layer of complexity, underscoring the need for a deeper understanding of the electronic structure in these multicomponent group-IV systems.

Previous studies have primarily focused on specific Sn compositions or incremental cavity design improvements, providing limited guidance for active-medium engineering based on fundamental physics. Here, we investigate an epitaxially grown GeSn/GeSn (x > y) multi-quantum-well heterostructure as the laser active medium across multiple strain configurations, highlighting electronic band-structure engineering as the main factor controlling optical emission. To this end, two distinct cavity designs are fabricated on both major technology platforms—on Ge virtual substrates **o**n-**S**i bulk (OS) and **o**n-**I**nsulator (OI)—serving as complementary strain-engineering strategies. By simultaneously tracking the evolution of emission spectra from spontaneous emission at cryogenic temperatures to room-temperature lasing, along with the temperature dependence of the lasing threshold, we reveal the key band-structure mechanisms governing efficient group-IV laser operation. These results underscore the critical interplay among moderate Sn content, strain control, and defect mitigation, establishing GeSn-on-insulator MQW microcavities as a robust, CMOS-compatible platform for mid-infrared on-chip light sources.

2 | Epitaxial Growth and Characterization of GeSn MQW Architecture

The GeSn-based heterostructures were epitaxially grown in an industrial reduced-pressure chemical vapor deposition (RP-CVD) reactor on Ge/Si virtual substrates, consisting of a 300 nm Ge heteroepitaxial layer deposited on 200 mm Si(100) wafers. A compositionally graded GeSn buffer was subsequently grown, in which the Sn content was progressively increased from 11 at.% to 14 at.% and then slightly reduced to ~12 at.%. The resulting ~ 300 nm-thick buffer promotes in situ strain relaxation, establishing an expanded in-plane lattice constant that serves as a template for the growth of the optically active multiple-quantum-well (MQW) stack. The MQW region consists of five periods of alternating GeSn layers, with 37 nm $Ge_{0.85}Sn_{0.15}$ wells and 13 nm $Ge_{0.90}Sn_{0.10}$ barriers. The first well, grown directly on the graded GeSn buffer terminating at 12 at.% Sn, is lattice-matched and exhibits a smaller band offset compared with the subsequent wells. The modulation of Sn composition between wells and barriers was achieved isothermally by adjusting the N_2 carrier gas flow in the reactor, following the methodology detailed in Ref. [29]. This growth approach ensures sharp compositional interfaces, minimal Sn segregation, and high reproducibility of the GeSn MQW heterostructure.

A comprehensive structural characterization of the epitaxial GeSn-based MQW heterostructure has been performed. Figure 1a presents high-resolution transmission electron microscopy (HR-TEM) images acquired at different magnifications, together with the corresponding two-dimensional Sn distribution maps obtained by energy-dispersive X-ray (EDX) analysis. These combined data sets confirm the high crystalline quality of the structure and the well-defined atomic-scale distribution of Sn across the MQW stack. These measurements reveal sharp, dislocation-free interfaces between wells and barriers, as well as abrupt Sn composition changes across the heterointerfaces. Such abruptness is critical for carrier confinement and optical gain in the MQW active region. Additionally, full-stack SIMS data, Figure 1b, show that the Sn concentrations remain close to the nominal values of 15 at.% for the wells and 10 at.% for the barriers. High-resolution x-ray reciprocal space mapping (RSM) around the (224) reflection, Figure 1c, confirms the pseudomorphic epitaxy of the MQW stack on the underlying GeSn buffer layer. While the 300 nm—thick Ge layer is slightly compressively strained +0.15%, the GeSn buffer is about 80% strain relaxed (close to the cubic line in reciprocal space). The $Ge_{0,85}Sn_{0.15}$ wells exhibit residual biaxial compressive strain of approximately −0.4 % and the $Ge_{0.9}Sn_{0.1}$ barriers are +0.23 % tensely strained. Both the wells and the barriers are direct bandgap semiconductors. Electronic band structure of the as-grown heterostructures, calculated at 5 K using a strain-resolved eight-band $k{\cdot}p$ model reveals that both the wells and the barriers are direct bandgap semiconductors and that they feature a type-I band alignment with both Γ—electrons and heavy holes (HH) confined and quantized in the $Ge_{0,85}Sn_{0.15}$ wells, (Figure 1c). Temperature-dependent photoluminescence (PL) emission spectra measured between 5 and 300 K are shown in Figure 1f. At 5 K, a strong

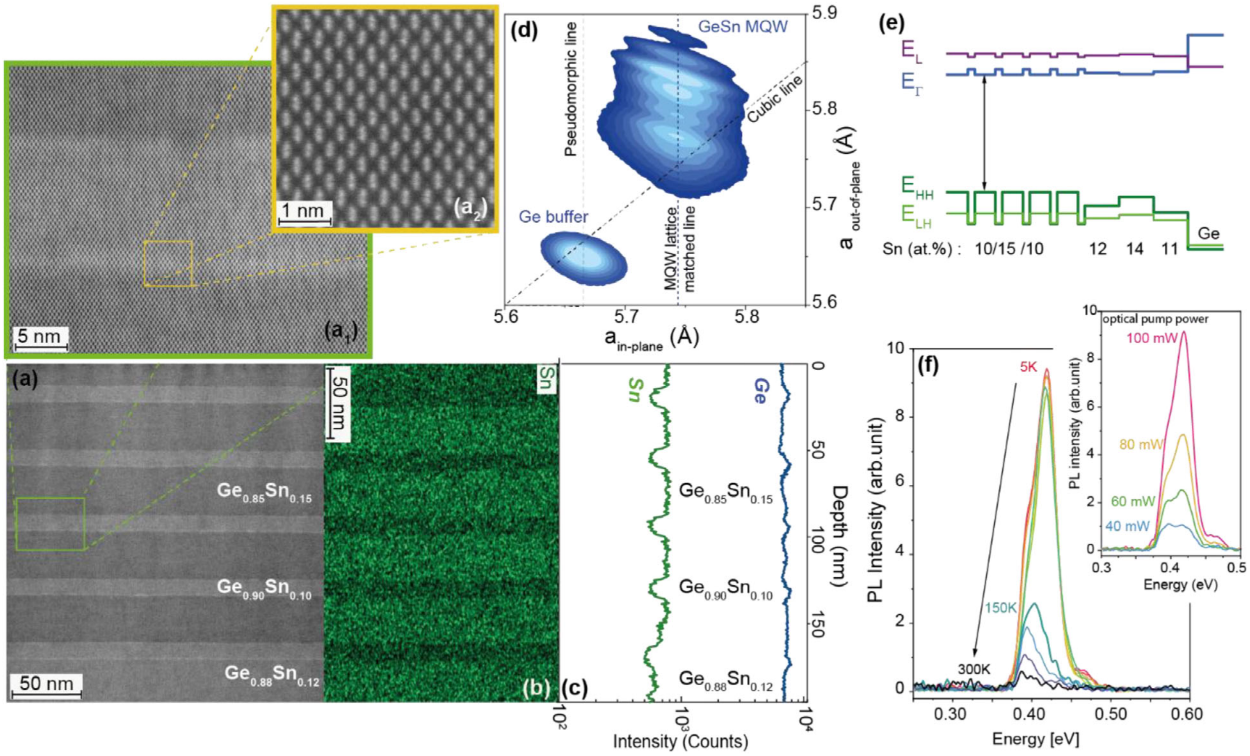

FIGURE 1 | Material characterization of the $Ge_{0.85}Sn_{0.15}/Ge_{0.90}Sn_{0.10}$ MQW heterostructure: (a) TEM image showing high crystalline quality and smooth well–barrier interfaces. Insets (a_1) and (a_2) show a single well and a high-resolution zoom inside the well, respectively. (b) EDX map showing the Sn elemental distribution. (c) SIMS profiles of Sn and Ge showing clear elemental modulation across the epitaxial stack. (d) X-ray RSM around the (224) reflection confirming pseudomorphic growth of the MQW stack. (e) Calculated electronic band structure of the MQW heterostructure. (f) Temperature dependent PL spectra and PL at 5 K under different electrical current densities.

emission peak is observed at approximately 0.442 eV, in excellent agreement with the calculated bandgap of 0.44 eV. The emission intensity decreases significantly above 150 K, which is attributed to thermally activated nonradiative recombination processes, possibly enhanced by carrier escape from the quantum wells, indicating limited carrier confinement and suggesting a relatively small band offset. Meanwhile, the linewidth exhibits only slight thermal broadening, increasing from about 30 meV at 5 K to 40 meV at 250 K, as expected for high-quality multiple quantum well (MQW) structures. The excitation power dependence of the PL at 5 K is presented in the inset of Figure 1f.

3 | The Laser Cavities

To evaluate the laser emission performances of the $Ge_{0.85}Sn_{0.15}/Ge_{0.90}Sn_{0.10}$ MQW heterostructure, four circular laser cavities were fabricated using two designs: mesa- and under-etched—type cavities. These were implemented on two different material platforms: on Si (OS) and on-insulator (OI) wafers. The OS platform involves direct patterning of the as-grown heterostructure (Figure 2a,b), whereas the OI platform is based on the patterning of a GeSn-based layers stack transferred onto an insulating buffered Si wafers via a layer-transfer process (Figure 2c,d). This latter architecture, commonly referred to as GeSn-on-insulator (GeSnOI), also facilitates the integration of additional interlayers between the insulator and the Si wafer. In this work, the insulating layer is a 400 nm SiN_x layer, which also acts as a stressor layer, inducing biaxial tensile strain in the GeSn cavity through processing and under-etching [9, 10, 30]. The additional interlayer is a thick Al layer, which has been shown in previous studies to reduce the laser cavity temperature by ∼ 10–15 K [19]. This architecture not only addresses key limitations of GeSn and Ge semiconductors and provides a scalable pathway for performance optimization. Scanning electron microscopy (SEM) imaging of the fabricated 8 µm diameter cavities reveals well-defined circular geometries with vertical and smooth sidewalls on both the bulk and GeSnOI platforms. These observations confirm the structural integrity and reproducibility of the fabrication process, as reported in Refs. [22, 31]

This work focuses on the influence of the electronic band structure on lasing performance. To achieve end, different cavities and platforms are employed to systematically tune the GeSn MQW strain from biaxial compressive to biaxial tensile, thereby controlling the band structure at the disk periphery where optical whispering-gallery modes (WGMs) are confined. In the mesa cavity on Si (mGeSnOS) the quantum wells retain their as-grown biaxial compressive strain, which lifts the valence-band degeneracy and positions the heavy-hole (HH) band as the top valence band. In under-etched cavity on Si (µ-GeSnOS), partial strain relaxation occurs in the suspended peripheral region of the disks [32], slightly improving the Γ – L directness while preserving the HH character of the valence band. In contrast, in the under-etched GeSn-on-insulator (µ-GeSnOI) cavity, the all-around SiN stressor layer induces biaxial tensile strain, leading to strong bandgap narrowing, enhanced Γ—L directness, and,

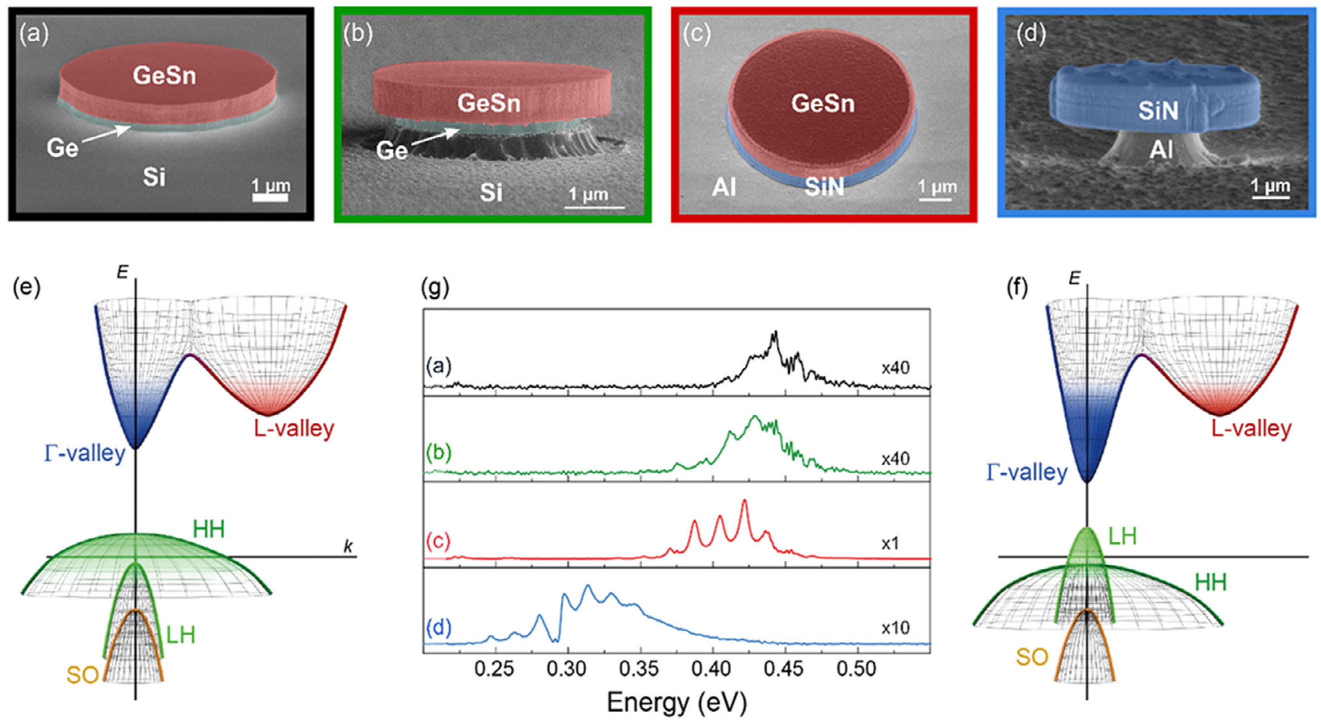

FIGURE 2 | Microdisk laser cavities: (a–d) SEM images of the fabricated GeSn MQW microdisk laser cavities: (a) mesa GeSn MQW on Si bulk (m-GeSnOS) ; (b) under-etched GeSn MQW on Si bulk (μ-GeSnOS) ; (c) mesa GeSn MQW on insulator (m-GeSnOI), and (d) under-etched GeSn MQW on insulator (μ-GeSnOI). (e,f) Schematic band diagrams illustrating the energy band alignment for mGeSnOS and μ-GeSnOI, respectively. (g) Emission spectra taken at 77 K for all cavity types, showing the emergence of whispering-gallery modes (WGMs and emission energy shift for different cavity configuration.

importantly, a valence-band reordering in which the light-hole (LH) band becomes the valence-band maximum. The electronic band structures for the biaxial compressive and tensile cases are schematically shown in Figure 2e,f, respectively, highlighting the inversion of the heavy-hole (HH) and light-hole (LH) bands in the valence band.

The strain variation is directly evidenced by photoluminescence (PL) measurements, as reflected in the energy shifts of the whispering-gallery modes (WGMs). Figure 2g presents the emission spectra acquired under continuous-wave excitation at 1.55 μm, showing a ∼ 15 meV redshift for the under-etched cavity relative to the mesa cavity on the bulk Si platform, and a significantly larger ∼ 100 meV redshift for the under-etched cavity on the insulator platform (μ-GeSnOI). These pronounced shifts demonstrate the effectiveness of strain engineering in tailoring the optical response of group-IV laser cavities. The emergence of sharper WGMs in the GeSnOI platform stems from enhanced optical confinement within the cavity, which suppresses scattering losses and, thereby, increases the quality factor.

4 | GeSn MQW Lasers on Si Bulk (GeSnOS) Platform

The fabricated laser cavities were characterized under optical pumping using a pulsed laser source with a central wavelength of 1.55 μm and a pulse width of 2 ns. The emission spectra of 8 μm diameter mesa and under-etched cavities fabricated on as-grown wafers are presented in Figure 3 and their 3D sketches are shown as insets. The optical emission was measured at 77 K under various pump power densities ranging from 450 to 6500 kW cm^{-2}. For the mesa cavity the spectral response consists only of spontaneous emission without any threshold behavior indicative of lasing even under high-excitation conditions.

A markedly different behavior is observed for the under-etched cavities. A sharp optical resonance at ∼ 0.46 eV emerges once the pump fluence exceeds 110 kW cm^{-2}, indicating the onset of stimulated emission. The lasing threshold, extracted from the inflection point of the light-in – light-out (L–L) characteristic, corresponds to the pump density at which the optical gain surpasses total cavity losses. A more rigorous threshold determination is obtained from the second derivative of the L–L curve, where a pronounced peak marks the transition from spontaneous to stimulated emission; this approach remains valid for both single- and multi-mode onset as long as a nonlinear change in output power occurs. The first lasing mode exhibits a threshold of 110 kW cm^{-2}. With Further increase in pump fluence, the device undergoes mode competition, starting at about 210 kW cm^{-2}: the initial lasing mode is quenched, while a higher-energy mode emerges and dominates.

The superior lasing performance observed in the under-etched cavity compared to the mesa cavity is associated with three main factors: (i) enhanced directness resulting from strain relaxation in the suspended disk region, which increases the material gain; (ii) improved optical mode confinement due to the significantly

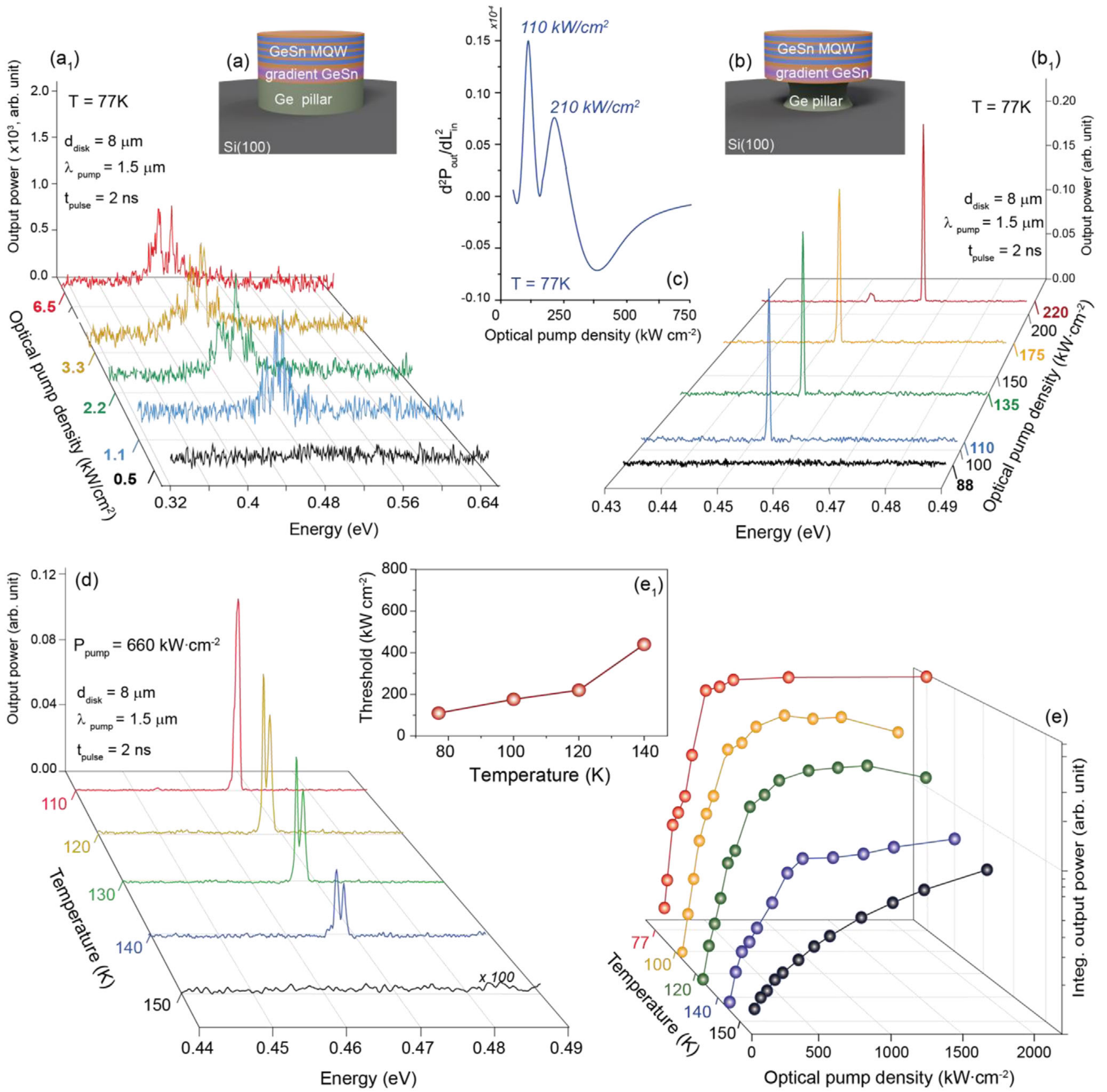

FIGURE 3 | GeSn MQW microdisk cavities on Si: (a) 3D schematic of the mesa GeSn MQW cavity on Si bulk (mGeSnOS). (a_1) Emission spectra of an 8 μm diameter mGeSnOS cavity under pulsed optical excitation, showing no evidence of lasing. (b) 3D schematic of the under-etched GeSn MQW cavity on Si bulk (μ-GeSnOS). (b_1) Emission spectra of an 8 μm diameter μ-GeSnOS cavity under increasing pulsed pump power, exhibiting single-mode lasing at threshold that transitions to multimode operation at higher excitation levels. (c) Second derivative of the L–L characteristic used to extract lasing thresholds. The first and second lasing modes exhibit thresholds of ∼110 and ∼210 kW cm^{-2}, respectively. (d) Temperature-dependent PL spectra under a constant excitation density of 600 kW cm^{-2}, showing sustained laser emission up to 140 K. (e) L–L characteristics used to determine temperature-dependent lasing thresholds, summarized in (e_1).

higher refractive index contrast at the GeSn/air interface ($\Delta n = 4.37$ at $\lambda = 3$ μm) compared with the GeSn/Ge interface ($\Delta n = 0.35$) [33, 34] and (iii) the removal in the under-etched WGM region of the highly defective heterointerface between the GeSn graded layer and the Ge buffer, which otherwise acts as a non-radiative recombination center [32]. Together, these factors enhance radiative carrier recombination and provide positive net optical gain, thereby facilitating lasing emission.

The maximum lasing operating temperature is a key figure of merit for laser performance. From the temperature—dependent emission spectra measured under a fixed pump excitation density of 660 kW cm^2 (Figure 4a), a maximum lasing operation temperature of 140 K is observed. The clear "S-shaped" of the L-L characteristics at low temperatures, showing the gain saturation regime following the initial exponential increase of the amplified emission, progressively flattens and becomes almost linear at

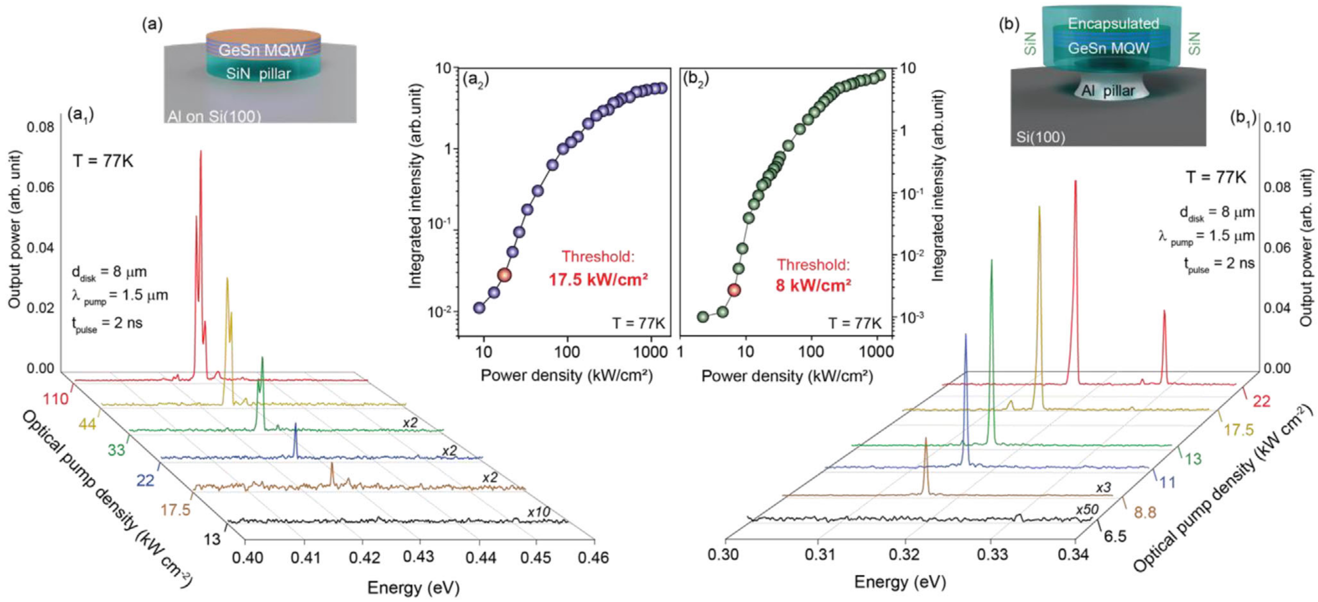

FIGURE 4 | GeSnOI MQW cavities at 77 K: (a) 3D sketch of the mGeSnOI laser cavity; (a_1) Emission spectra of an 8 µm diameter mGeSnOI cavity under pulsed laser operation under different optical pump powers and (a_2) its L–L characteristic indicating a 17.8 kW cm^{-2} lasing threshold. (b) shows a sketch of the µ-GeSnOI laser cavity, (b_1) Emission spectra of an 8 µm diameter µ-GeSnOI cavity under pulsed laser operation under different optical pump powers and (b_2) its L–L characteristic indicating an 8 kW cm^{-2} lasing threshold.

150 K, consistent with the disappearance of lasing as shown in Figure 3b. The laser threshold, extracted from the L–L characteristics, rises sharply from 110 kW cm^{-2} at 77 K to ~ 450 kW cm^{-2} at 140 K. This pronounced increase is attributed not only to thermal carrier scattering between the Γ- and L- valleys, as observed in bulk GeSn lasers, but also to quantum well-specific effects. In particular, carrier redistribution into higher-energy sublevels within the quantum wells with reduced optical gain and carriers escape over the quantum well band offset, further lower the population inversion and contribute to the increased threshold.

5 | Strain Engineered GeSn MQW Lasers on OI Platform

The GeSn on-Insulator technology has been shown to significantly enhance the performance of thick GeSn bulk lasers [9, 10, 19, 20]. Herein, a complex GeSn-based MQW heterostructure is transferred onto a receiver wafer. Figure 4a,b schematically show the MD laser cavities whose properties are directly compared to those of the mesa and under-etched GeSnOS. The under-etched cavities (µ-GeSnOI) are fabricated by selectively etching the Al layer beneath the cavity, a process that induces biaxial tensile strain in the GeSn MQW layer by relaxing the compressive strain in the SiN_x stressor layer underneath. To ensure a uniform tensile strain distribution throughout the GeSn MQW stack, the entire cavity is encapsulated with a 400 nm thick SiN_x layer. Further fabrication details can be found in Ref. [10]. The optical emission spectra at 77 K for mesa (mGeSnOI) and under-etched (µ-GeSnOI) cavities, measured under the same optical conditions as the GeSnOS counterparts, are presented in Figure 4a_1,b_1.

In contrast to the mGeSnOS (Figure 3a), where only weak spontaneous emission is observed, the mGeSnOI cavity exhibits strong, well-defined laser emission. Multimode lasing occurs e.g., under a pump density of 110 kW cm^{-2}, indicating broad and high optical gain. From the L–L characteristic at 77 K (Figure 4a_2), a lasing threshold of ~17.6 kW cm^{-2} is extracted. This threshold, lower than that reported for bulk GeSn with comparable [9] or even lower Sn content [19], is attributed to carrier quantization, which reduces the required population inversion, and to carrier confinement within the MQWs, which suppresses diffusion losses and promotes efficient radiative recombination. In contrast to the laser cavities on bulk Si, the key distinction here arises from the complete removal of the partially relaxed GeSn graded buffer and its dislocated interface with the Ge layer, leaving only the high-quality crystalline GeSn MQW stack transferred onto the receiver wafer. The improvement in cavity quality factor is already evident from the WGM spectra shown in Figure 2.

The emission spectra at 77 K of the µ-GeSnOI cavity are shown in Figure 4b_1. Pump power–dependent measurements show single-mode lasing that transitions to multimode emission above ~22 kW cm^{-2}. This behavior reflects a broadening of the optical gain spectrum with increasing carrier injection, enabling population inversion over a wider spectral range; as the excitation density rises, higher-order whispering-gallery modes (WGMs) reach the lasing threshold, giving rise to the observed multimode emission. From the L–L characteristic, presented in Figure 4b_2 a lasing threshold of 8 kW cm^{-2} at 77 K is extracted using the second derivative method. This threshold is 50% lower compared with the mGeSnOI cavity and an order of magnitude lower than the µ-GeSnOS counterpart. Notably, this threshold is also lower than any previously reported values for GeSn cavities of any geometry or alloy composition, including both bulk and MQW devices [19].

The enhanced performance of the tensile-strained µ-GeSnOI cavities arises from the synergistic interplay between band structure engineering and cavity design. Biaxial tensile strain favors the direct Γ → LH transition, which has larger transition matrix

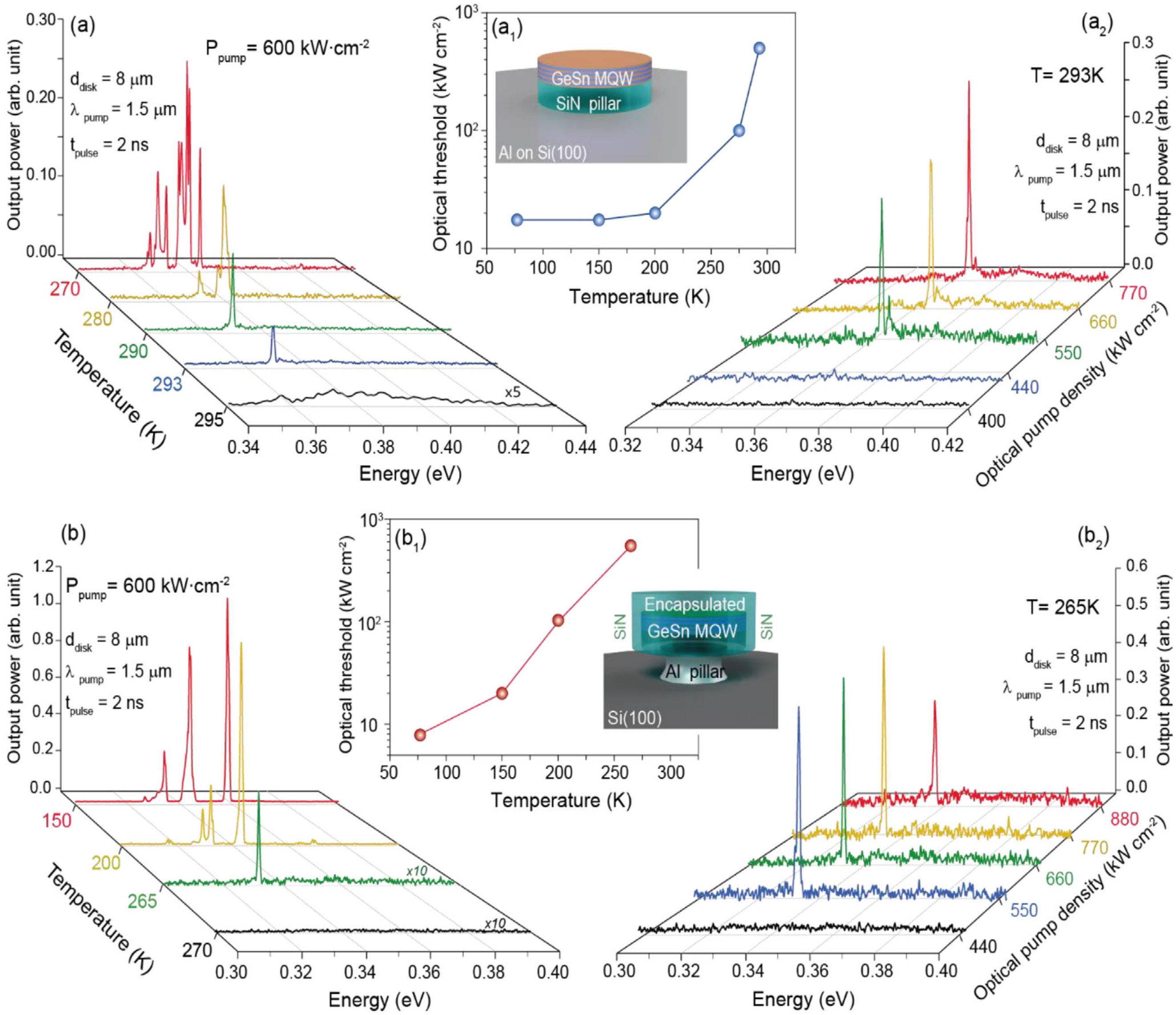

FIGURE 5 | GeSnOI MQW cavities at elevated temperatures: Emission spectra of a (a) mesa GeSnOI (mGeSnOI) and (b) under-etched GeSnOI (µ-GeSnOI) cavities under a constant optical pump of 660 kW cm^{-2} as a function of temperature. Temperature dependence of the lasing threshold for the (a_1) mGeSnOI cavity and (b_1) µ-GeSnOI cavity. PL spectra of the (a_2) mGeSnOI cavity at 293K and (b_2) µ-GeSnOI cavity at 265K under different pump powers.

elements than the less favorable Γ → HH transition in other strain configurations. This increases optical gain and lowers the carrier density required to reach the lasing threshold, owing to the reduced density of states in both the Γ- and LH bands [10, 35]. As mentioned above, tensile strain further increases the material's directness by lowering the Γ-valley energy, suppressing intravalley scattering, and narrowing the bandgap. At 77 K, the emission redshifts to ~3.9 µm (~0.318 eV), compared with ~2.9 µm (~0.428 eV) in unstrained material, demonstrating that biaxial tensile strain provides an effective handle to tune the laser emission wavelength in GeSn MQWs.

The temperature-dependent emission spectra of both mesa (mGeSnOI) and under-etched (µ-GeSnOI) cavities are shown in Figure 5 for a pump density of 660 kW cm^{-2}, well above threshold. At low and intermediate temperatures, both cavities exhibit multimode lasing, which gradually evolves into single-mode operation before lasing is quenched. This transition reflects the combined effect of (i) reduced overlap between the optical gain spectrum and the WGM cavity modes, and (ii) the decreased quality factors of higher-order modes due to increased absorption and carrier scattering, allowing the dominant mode to prevail. This behavior underscores the delicate interplay between thermal effects and modal dynamics in group-IV lasers [9, 10, 19, 20]. Remarkably, the mGeSnOI cavity sustains lasing up to room temperature (293 K, ~ 20°C), constituting, to our knowledge, the first demonstration of room-temperature lasing from a GeSn multiple quantum well heterostructure. For the under-etched µ-GeSnOI cavity, a maximum lasing temperature of only 265 K is reached. Although this value exceeds that of previously reported GeSnOI lasers [10, 19], it remains below the lasing temperature of the mGeSnOI cavity. The temperature-dependent lasing thresholds of GeSn MQW microdisk lasers on bulk and insulator platforms show distinct behaviors. The bulk

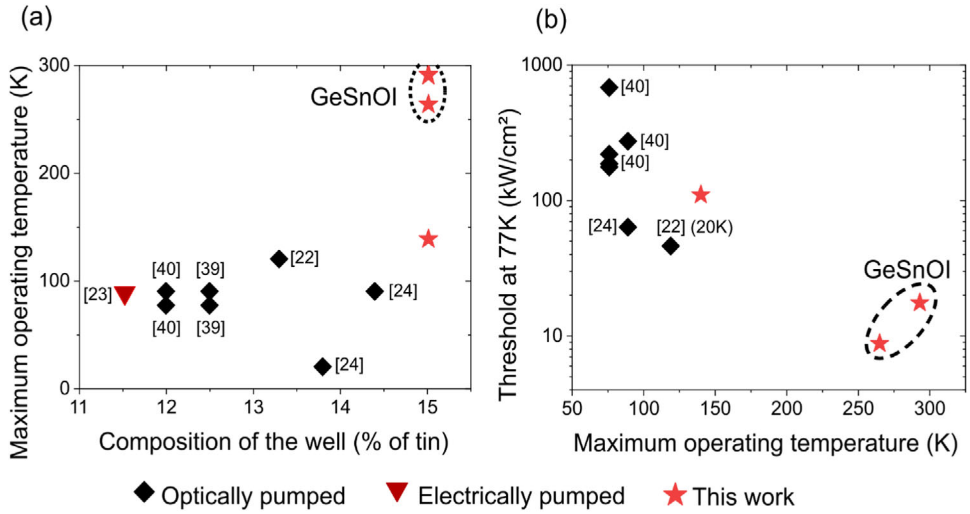

FIGURE 6 | Benchmark Exclusively Dedicated to GeSn QW lasers: (a) Maximum operating temperature versus the Sn content in the quantum well. (b) Threshold at cryogenic temperature versus maximum operating temperature. Near each previously reported performance, the corresponding references are indicated [22–24, 39, 40].

device (μ-GeSnOS) exhibits a uniform threshold increase with temperature, corresponding to a nearly constant characteristic temperature of T_0 ~70 K (Figure 3e_1), indicative of moderate but stable thermal sensitivity. In contrast, the m-GeSnOI laser displays a nearly temperature-independent threshold up to 200 K (Figure 5a_1), corresponding to an effectively infinite T_0, followed by a pronounced transition where the threshold rises rapidly, yielding T_0 ~30–40 K. A similar two-regime behavior is observed for the tensile-strained μ-GeSnOI: an enhanced low-temperature performance with T_0 ~ 90 K between 80 and 150 K, followed by a strong degradation above ~150 K with T_0≈30 K (Figure 5b_1). Notably, the onset of rapid threshold increase occurs at a lower temperature for the tensile strain case compared to the bulk structure, indicating an earlier activation of loss mechanisms. Overall, while strain engineering and improved carrier confinement significantly enhance low-temperature lasing performance, all non-bulk structures exhibit a pronounced reduction in T_0 at elevated temperatures, pointing to a common limitation governed by intrinsic recombination processes. Despite the 50% lower threshold for the tensile strained cavity at 77 K, both structures have indeed similar thresholds of ~ 500 kW cm^{-2}, at their maximum working temperature. This was already observed in the literature [9] also for bulk GeSn lasers and for different type of laser cavities. While a clear explanation is not presented it is supposed to be related with heat dissipation due to the low lattice thermal conductivity of GeSn [36–38]. Finally, for completeness, Figure 5a_2,b_2 presents the emission spectra as a function of excitation power at the maximum operating temperature of each cavity: 293 K for the mGeSnOI (Figure 5a_2), and 265 K for the μ-GeSnOI (Figure 5b_2).

6 | Discussions and Outlook

The literature reported figures-of-merit for GeSn-based quantum structures are benchmarked in Figure 6. The maximum operating temperature typically increases with the Sn content in the quantum wells, as expected by increasing the energy separation between the Gamma and the L-valley, reducing the carrier intra-valleys scattering. All the on Si bulk heterostructures present a reduced operation temperatures, with the current GeSn MQW structure containing 15 at.% Sn in the well, acgieving the highest temperate of 140 K. The on-insulator transferred GeSn-based MQW reached 265 and 293 K, depending on the cavity design, as shown above, highlighting the effectiveness of strain engineering combined with enhanced thermal management [22–24, 39]. Since no room-temperature lasing has been reported for GeSn quantum well structures to date, the laser threshold can only be compared at cryogenic temperatures. The μGeSnOI microdisk exhibits the lowest threshold value of 8 kW cm^{-2}, roughly 50% that of the mesa-type GeSnOI cavity and an order of magnitude lower than previous bulk-like structures with similar Sn content. Most prior laser studies provide only punctual insights, typically focusing on a specific Sn composition or isolated cavity design optimizations, with limited emphasis on the systematic, physics-driven engineering of the active medium. This advances the field by conducting a comprehensive investigation of the emission properties of GeSn MQW heterostructures with a primary focus on strain-driven band-structure tailoring. Technological enhancements to the laser architecture are treated as a secondary, enabling factor rather than the central design driver.

Optical mode confinement and heat dissipation undoubtedly influence the lasing behavior. A simple optical confinement analysis indicates that the optical mode overlap with the GeSn active region increases from approximately 30% for the mesa structure on bulk Si to approximately 90% for the underetched microdisk geometry, owing to the localization of the whispering-gallery mode within the suspended GeSn rim [33, 34]. For the GeSn-on-insulator platform consisting of GeSn on SiN on Al, the GeSn layer forms the highest-index region of the structure, while the SiN layer provides strong optical confinement and the Al layer suppresses downward optical leakage through reflection, resulting in an estimated optical mode overlap of approximately 70% even without underetching. In contrast to the bulk-Si platform, underetching is therefore not expected to provide a substantial additional improvement in optical confinement, as the whispering-gallery modes are already predominantly localized within the outer suspended region of the GeSn active layer. Thermal management also plays an important role: the mGeSnOI cavity is fully supported by an Al layer, an efficient thermal conductor, and therefore operates at temperatures approximately 10–15 K [19] higher than the μ-GeSnOI cavity, where heat is extracted only through a narrow Al pedestal. Although both optical confinement and thermal effects contribute to the observed performance differences, they cannot fully explain the markedly different lasing thresholds or, more surprisingly, why the tensile-strained MQW cavities cease lasing at lower temperatures despite the intuitive expectation of improved performance under tensile strain.

The origin of this behavior lies in the strain- and temperature-dependent electronic band structure of the GeSn MQW heterostructure. In tensile-strained GeSn, the combined effects of Sn composition and biaxial strain can bring the inter-band Γ–LH transition into resonance with intra-valence-band (IVB) transitions involving the HH, LH, and split-off (SO) bands [2]. This resonance introduces parasitic absorption (i.e., negative optical gain), which competes with and ultimately suppresses stimulated emission, thereby limiting the lasing temperature despite the nominally favorable band structure under tensile strain.

In GeSn-based MQW structures, this situation becomes even more intricate: both wells and barriers are direct-gap semiconductors whose strain states concurrently reshape their electronic band structures. Consequently, in addition to standard emission and absorption within the wells, resonant coupling can occur in which photons emitted from the wells are reabsorbed in the barriers. Using standard deformation-potential estimates, tensile biaxial strains of a few-tenths of a percent up to ∼ 1 % can produce valence-band splitting and band-edge shifts of 10–100 meV (see Figure 5) precisely the energy range needed for a Γ → LH transition in the well to resonate with intra-valence band transitions in the barrier. For quantum structure specifically, the band offsets between the wells and barriers are an additional degree of freedom that strongly influences the lasing behavior. The complexity is further enhanced by the strong temperature dependence of the band structure.

A fully comprehensive treatment of the coupled strain–composition–quantization–temperature interactions in GeSn-based MQW heterostructures is beyond the scope of this work. Accurately determining the strain conditions that induce resonance requires full *k·p* or *ab-initio* modeling that incorporates band offsets, alloy bowing, quantum confinement, and the temperature dependence of both electronic energies and lattice strain. Looking ahead, machine-learning–assisted band-structure frameworks provide a promising pathway to efficiently optimize GeSn/GeSn MQWs for low-threshold, room-temperature lasing.

The recent availability of reliable material parameters for GeSn alloys—including Γ-valley electron effective masses [41], hole effective masses, Luttinger parameters [42], and lattice thermal conductivities [36–38] – together with continued advances in group-IV epitaxy, now enables the realization of sophisticated quantum-well architectures based on binary GeSn, ternary SiGeSn and GeSnC, and quaternary CSiGeSn alloys [18]. These developments open the door to data-driven, AI-guided design of next-generation group-IV laser heterostructures, achieving unprecedented precision while bridging fundamental band-structure physics with scalable, CMOS-compatible photonic platforms. Nevertheless, fully exploiting these capabilities will require the coordinated integration of experimental validation, strain-engineering methodologies, and thermal-management strategies to translate computational insights into high-performance devices.

7 | Conclusion

In this work, a comparative investigation of GeSnx/GeSny multi-quantum-well (MQW) lasers on both bulk-Si and on-insulator platforms is presented, establishing explicit links between heterostructure design, strain state, and laser performance. On bulk Si, GeSn MQW microdisk cavities exploit whispering-gallery modes to achieve strong optical confinement and low lasing thresholds at cryogenic temperatures; however, defective interfaces and limited heat dissipation restrict operation to temperatures below ∼140 K. In contrast, the layer-transfer on-insulator platform enables strain-driven band-structure engineering together with improved thermal management through Al interlayers. This approach yields the first demonstration of room-temperature lasing in a GeSn-based MQW system and, in partially suspended microdisk cavities, ultralow thresholds of 8 kW cm^{-2} at 77 K. The extension of laser emission to ∼3.9 μm, well beyond the range accessible to other silicon-based light sources, further expands the application space of group-IV photonics toward mid-infrared sensing, spectroscopy, and free-space communication.

These results highlight the importance of the interplay between band-structure engineering, strain management, optical confinement, and thermal dissipation in determining the performance of GeSn MQW lasers. The combination of low-threshold operation, extended wavelength coverage, and room-temperature lasing positions the GeSn-on-insulator MQW platform among the most promising group-IV laser technologies reported to date. While further refinement through advanced band-structure modeling is required to optimize the balance between optical gain and resonant absorption, the present work establishes GeSn-based heterostructures as a promising platform for energy-efficient and scalable mid-infrared lasing. By bridging the gap between cryogenic and room-temperature operation, these results contribute to the ongoing development of silicon-photonics-compatible light sources and integrated group-IV photonic systems.

Acknowledgements

The authors acknowledge financial support from the European Commission for the LASTSTEP Project under grant agreement 101070208 and the German Federal Ministry of Research, Technology, and Space via the GFORLASER project, No. 13N17312. The authors acknowledge for funding from the French research agency grant through MAGIQ-ANR20-CE24-0027 project and support from the French RENATECH network.

Open access funding enabled and organized by Projekt DEAL.

Author Contributions

Antoine Meyer: data curation, visualization, investigation, writing original draft, formal analysis, validation. **Hector-Mauricio Reynoso-de la Cruz:** investigation, data curation, formal analysis, writing original draft, visualization, validation. **Omar Concepción:** conceptualization, data curation, validation, methodology. **Prateek Kaul:** data curation, validation. **Konstantinos Pantzas:** data curation, validation, resources. **Etienne Herth:** methodology, investigation, resources, validation, writing original draft. **Z. Ikonic:** conceptualization. **Giovanni Capellini:** methodology, conceptualization, validation. **Detlev Grützmacher:** validation, project administration. **Moustapha El Kurdi:** validation, methodology, conceptualization, writing original draft, funding acquisition, investigation, supervision, formal analysis, visualization, resources. **Dan Buca:** funding acquisition, validation, writing original draft, conceptualization, methodology, investigation, supervision, formal analysis, visualization, resources.

Conflicts of Interest

The authors declare no conflicts of interest.

Data Availability Statement

All data generated and analyzed during the present study are included in this article and are available from the corresponding author upon reasonable request. Data originating from previously published work are cited in the reference list.

References

1. O. Moutanabbir, S. Assali, X. Gong, et al., "Monolithic Infrared Silicon Photonics: The Rise of (Si)GeSn Semiconductors," *Applied Physics Letters* 118 (2021): 110502, https://doi.org/10.1063/5.0043511.

2. R. Soref, D. Buca, and S.-Q. Yu, "Group IV Photonics: Driving Integrated Optoelectronics," *Optics Photonics News* 27 (2016): 32–39.

3. D. Lee, M. Park, Y. Baek, B. Bae, J. Heo, and K. Lee, "In-sensor Image Memorization and Encoding via Optical Neurons for Bio-Stimulus Domain Reduction Toward Visual Cognitive Processing," *Nature Communications* 13 (2022): 5223, https://doi.org/10.1038/s41467-022-32790-3.

4. C. Ríos, N. Youngblood, Z. Cheng, et al., "In-Memory Computing on a Photonic Platform," *Science Advances* 5 (2019): aau5759.

5. H.-K. Peng, Y.-K. Huang, C.-P. Chou, and Y.-H. Wu, "Recognizing Spatiotemporal Features by a Neuromorphic Network With Highly Reliable Ferroelectric Capacitors on Epitaxial GeSn Film," *ACS Applied Materials & Interfaces* 13 (2021): 26630–26638, https://pubs.acs.org/doi/10.1021/acsami.1c05815.

6. N. Von Den Driesch, D. Stange, S. Wirths, et al., "Direct Bandgap Group IV Epitaxy on Si for Laser Applications," *Chemistry of Materials* 27 (2015): 4693–4702.

7. W. Dou, M. Benamara, A. Mosleh, et al., "Investigation of GeSn Strain Relaxation and Spontaneous Composition Gradient for Low-Defect and High-Sn Alloy Growth," *Scientific Reports* 8 (2018): 5640, https://doi.org/10.1038/s41598-018-24018-6.

8. D. Stange, S. Wirths, R. Geiger, et al., "Optically Pumped GeSn Microdisk Lasers on Si," *ACS Photonics* 3 (2016): 1279–1285, https://doi.org/10.1021/acsphotonics.6b00258.

9. D. Buca, A. Bjelajac, D. Spirito, et al., "Room Temperature Lasing in GeSn Microdisks Enabled by Strain Engineering," *Advanced Optical Materials* 10 (2022): 2201024, https://doi.org/10.1002/adom.202201024.

10. A. Elbaz, D. Buca, N. von den Driesch, et al., "Ultra-Low-Threshold Continuous-Wave and Pulsed Lasing in Tensile-Strained GeSn Alloys," *Nature Photonics* 14 (2020): 375–382, https://doi.org/10.1038/s41566-020-0601-5.

11. J. Cui, J. Zheng, J. Li, et al., "Broadband Shortwave Infrared GeSn Light-Emitting Diode at Room Temperature Fabricated by Exploring the Sn Content Gradient Method," *Optics Letters* 50 (2025): 4142–4145, https://doi.org/10.1364/OL.561592.

12. V. Singh, P. T. Lin, N. Patel, et al., "Mid-Infrared Materials and Devices on a Si Platform for Optical Sensing," *Science and Technology of Advanced Materials* 15 (2014): 014603, https://doi.org/10.1088/1468-6996/15/1/014603.

13. M. Sieger and B. Mizaikoff, "Toward on-Chip Mid-Infrared Sensors," *Analytical Chemistry* 88 (2016): 5562–5573.

14. A. Elbaz, R. Arefin, E. Sakat, et al., "Reduced Lasing Thresholds in GeSn Microdisk Cavities With Defect Management of the Optically Active Region," *ACS Photonics* 7 (2020): 2713–2722, https://doi.org/10.1021/acsphotonics.0c00708.

15. S. Wirths, R. Geiger, N. von den Driesch, et al., "Lasing in Direct-bandgap GeSn Alloy Grown on Si," *Nature Photonics* 9 (2015): 88–92, https://doi.org/10.1038/nphoton.2014.321.

16. Y. Zhou, W. Dou, W. Du, et al., "Optically Pumped GeSn Lasers Operating at 270 K With Broad Waveguide Structures on Si," *ACS Photonics* 6 (2019): 1434–1441, https://doi.org/10.1021/acsphotonics.9b00030.

17. H.-J. Joo, Y. Kim, D. Burt, et al., "1D photonic Crystal Direct Bandgap GeSn-on-Insulator Laser," *Applied Physics Letters* 119 (2021): 201101, https://doi.org/10.1063/5.0066935.

18. Y. Kim, S. Assali, J. Ge, et al., "Mid-Infrared Group IV Nanowire Laser," *Science Advances* 11 (2025): adt6723, https://doi.org/10.1126/sciadv.adt6723.

19. B. Wang, E. Sakat, E. Herth, et al., "GeSnOI Mid-Infrared Laser Technology," *Light: Science & Applications* 10 (2021): 232, https://doi.org/10.1038/s41377-021-00675-7.

20. A. Bjelajac, M. Gromovyi, E. Sakat, et al., "Up to 300 K Lasing With GeSn-On-Insulator Microdisk Resonators," *Optics Express* 30 (2022): 3954–3961, https://doi.org/10.1364/OE.449895.

21. D. Stange, N. von den Driesch, D. Rainko, et al., "Short-Wave Infrared LEDs From GeSn/SiGeSn Multiple Quantum Wells," *Optica* 4 (2017): 185–188, https://doi.org/10.1364/OPTICA.4.000185.

22. D. Stange, N. von den Driesch, T. Zabel, et al., "GeSn/SiGeSn Heterostructure and Multi Quantum Well Lasers," *ACS Photonics* 5 (2018): 4628–4636, https://doi.org/10.1021/acsphotonics.8b01116.

23. L. Seidel, T. Liu, O. Concepción, et al., "Continuous-wave Electrically Pumped Multi-Quantum-Well Laser Based on Group-IV Semiconductors," *Nature Communications* 15 (2024): 10502, https://doi.org/10.1038/s41467-024-54873-z.

24. J. Margetis, Y. Zhou, W. Dou, et al., "All Group-IV SiGeSn/GeSn/SiGeSn QW Laser on Si Operating up to 90 K," *Applied Physics Letters* 113 (2018): 221104, https://doi.org/10.1063/1.5052563.

25. O. Concepción, A. J. Devaiya, M. H. Zoellner, et al., "Adaptive Epitaxy of C-Si-Ge-Sn: Customizable Bulk and Quantum Structures (Adv. Mater. 37/2025)," *Advanced Materials* 37 (2025): 70506, https://doi.org/10.1002/adma.70506.

26. L. M. Vogl, S. Chen, P. Schweizer, et al., "Identification of Short-Range Ordering Motifs in Semiconductors," *Science* 389 (2025): 1342–1346, https://doi.org/10.1126/science.adu0719.

27. S. Gougam, F. De Angelis, C. Meneghini, et al., "EXAFS Sheds Light on Short-Range Ordering in $Ge_{1-x}Sn_x$ Heteroepitaxial Layers Grown by MBE and CVD," *Physical Review Materials* 9 (2025): 064601, https://doi.org/10.1103/PhysRevMaterials.9.064601.

28. S. Mukherjee, N. Kodali, D. Isheim, et al., "Short-range Atomic Ordering in Nonequilibrium Silicon-Germanium-Tin Semiconductors," *Physical Review B* 95 (2017): 161402, https://doi.org/10.1103/PhysRevB.95.161402.

29. O. Concepción, N. B. Søgaard, J.-H. Bae, et al., "Isothermal Heteroepitaxy of $Ge_{1-x}Sn_x$ Structures for Electronic and Photonic Applications," *ACS Applied Electronic Materials* 5 (2023): 2268–2275, https://doi.org/10.1021/acsaelm.3c00112.

30. A. Ghrib, M. El Kurdi, M. Prost, et al., "All-Around SiN Stressor for High and Homogeneous Tensile Strain in Germanium Microdisk Cavities," *Advanced Optical Materials* 3 (2015): 353–358, https://doi.org/10.1002/adom.201400369.

31. V. Reboud, O. Concepción, W. Du, et al., "Advances in GeSn Alloys for MIR Applications," *Photonics and Nanostructures—Fundamentals and Applications* 58 (2024): 101233, https://doi.org/10.1016/j.photonics.2024.101233.

32. C. Corley-Wiciak, M. H. Zoellner, A. A. Corley-Wiciak, et al., "Full Picture of Lattice Deformation in a $Ge_{1-x}Sn_x$ Micro-Disk by 5D X-ray Diffraction Microscopy," *Small Methods* 8 (2024): 2400598, https://doi.org/10.1002/smtd.202400598.

33. J. H. Burnett, S. G. Kaplan, E. Stover, and A. Phenis, "Refractive Index Measurements of Ge," in *Infrared Sensors, Devices, and Applications VI*, vol. 9974 (SPIE, 2016), 222–232.

34. H. Tran, W. Du, S. A. Ghetmiri, et al., "Systematic Study of Ge1−xSnx Absorption Coefficient and Refractive Index for the Device Applications of Si-Based Optoelectronics," *Journal of Applied Physics* 119 (2016): 103106, https://doi.org/10.1063/1.4943652.

35. D. Rainko, Z. Ikonic, A. Elbaz, et al., "Impact of Tensile Strain on Low Sn Content GeSn Lasing," *Scientific Reports* 9 (2019): 259, https://doi.org/10.1038/s41598-018-36837-8.

36. P. Graziosi, D. Marian, A. Tomadin, et al., "Epitaxial SiGeSn Alloys for CMOS-Compatible Thermoelectric Devices," *ACS Applied Energy Materials* 8 (2025): 9075–9082, https://doi.org/10.1021/acsaem.5c00733.

37. D. Spirito, N. von den Driesch, C. L. Manganelli, et al., "Thermoelectric Efficiency of Epitaxial GeSn Alloys for Integrated Si-Based Applications: Assessing the Lattice Thermal Conductivity by Raman Thermometry," *ACS Applied Energy Materials* 4 (2021): 7385–7392, https://doi.org/10.1021/acsaem.1c01576.

38. O. Concepción, J. Tiscareño-Ramírez, A. A. Chimienti, et al., "Room Temperature Lattice Thermal Conductivity of GeSn Alloys," *ACS Applied Energy Materials* 7 (2024): 4394–4401, https://doi.org/10.1021/acsaem.4c00275.

39. G. Abernathy, S. Ojo, J. M. Grant, et al., "Study of Critical Optical Confinement Factor for GeSn-based Multiple Quantum Well Lasers," *Applied Physics Letters* 121 (2022): 171101, https://doi.org/10.1063/5.0107081.

40. G. Abernathy, S. Ojo, A. Said, et al., "Study of All-Group-IV SiGeSn Mid-IR Lasers With Dual Wavelength Emission," *Scientific Reports* 13 (2023): 18515, https://doi.org/10.1038/s41598-023-45916-4.

41. P. Kaul, O. Concepción, D. H. Wielens, et al., "Phase-Coherent Transport in GeSn Alloys on Si," *Advanced Electronic Materials* 11 (2025): 2400565, https://doi.org/10.1002/aelm.202400565.

42. P. Kaul, J. Karthein, J. Buchhorn, et al., "GeSn Quantum Wells as a Platform for Spin-Resolved Hole Transport," *Communications Materials* 6 (2025): 216, https://doi.org/10.1038/s43246-025-00934-9.